

Establishing a Formation of Small Satellites in a Lunar Flower Constellation

Lauren McManus¹ · Hanspeter Schaub^{2,3}

Published online: 12 September 2016
© American Astronautical Society 2016

Abstract The success of previous lunar science missions can be expanded upon by using a constellation of satellites to increase the lunar surface coverage. A constellation could also serve as a communications or GPS network for a lunar human base. Small-sats, deployed from a single mothercraft, are proposed to achieve a lunar constellation. The establishment of a single- and multi-petal constellation is investigated where the mothercraft does the primary deployment maneuvers. The constellation lifetime and closed-loop maintenance are addressed once higher order lunar gravity fields and Earth/solar perturbations are included.

Keywords Lunar constellation · Small satellites · Flower constellation · Repeat groundtracks

Introduction

The *Vision and Voyages for Planetary Science in the Decade 2013-2022* report produced by the National Academy of Sciences states that the moon “provides data critical for understanding the formation and evolution of habitable worlds like our

✉ Lauren McManus
lauren.mcmanus@colorado.edu

¹ Aerospace Engineering Sciences, University of Colorado, Boulder, CO, USA

² Department of Aerospace Engineering Sciences, University of Colorado, Boulder, CO 431 UCB, USA

³ Center for Astrodynamics Research, Boulder, CO 80309-0431, USA

own” [1]. The moon, as well as the other inner planets, are critical to assessing how rocky planets form and change over time. The moon in particular is considered to be a key to deciphering the evolutionary history of planets because it preserves a surface record spanning most of solar system history and is very accessible from Earth [2]. In addition to lunar science missions, if humans were to return to the Moon and establish a lunar base, they would require a communication satellite structure. A small-satellite constellation at the Moon, deployed from a single mothercraft, is proposed as a configuration for potential science or communications missions. Small satellites, such as cubesats, are desired for this constellation due to their affordability.

A constellation at the Moon has never been established, but previous lunar missions that included formation flying were the Gravity Recovery and Interior Laboratory (GRAIL) from 2011-2012 and the Japanese Kaguya (SELENE) mission to the Moon from 2007-2009. The GRAIL mission had two identical satellites flying in a leader-follower formation, similar to the Earth based gravity field mapping mission known as GRACE [2]. The SELENE mission differs from GRAIL in that there were a total of three satellites, and the main orbiter carried the two subsatellites on its roof to the Moon where they were released into their own orbits [3]. These missions have used more traditionally sized spacecraft, rather than the small-sats proposed in this work. Some small-sat constellations have been flown successfully at Earth however, including the Flock constellation from Planet Labs [4] and QB50 [5].

Repeat groundtrack orbits offer interesting options for potential science or communication constellations, as they provide repeat coverage of the surface at a fixed time between sequential visits. This allows the sensors to revisit the same location of the celestial body and compare to the location specific data of an extended period of time with dense data coverage. Flower constellations are a particular family of J_2 -frozen repeat groundtrack constellations being studied by Daniele Mortari at Texas A&M University that utilize repeat groundtracks. Orbital parameters are selected such that the nodal period of the orbit matches the nodal period of the primary body by a factor dependent on the number of days to repeat and the number of revolutions to repeat the groundtrack. All orbits in a flower constellation have identical orbital elements, with the exception of the right ascension of the ascending node (RAAN) and the initial mean anomaly, which are determined based on the phasing scheme desired.

Flower constellations have thus far primarily been studied about Earth, and has resulted in a wealth of interesting constellation geometries. A flower constellation at the Moon could be quite useful for science or communications purposes. In this scenario, the flower constellation satellites would be small satellites, which introduces many unique challenges. The small-sats would have limited propulsion capability and would be deployed from a mothercraft in order to avoid large, fuel-expensive plane change maneuvers. Orbital maintenance would then be required after deployment to retain the J_2 -frozen repeat groundtrack nature of the flower constellation. The limited fuel on the small-sats and the maneuvers required determine the lifetime of the constellation. The communications range of the small-sats will also be limited, so that once the deployment is complete, the mothercraft must move into a longterm communications orbit where it can see the children craft as well as Earth, and act as a communications relay. A lunar flower constellation concept is shown in Fig. 1. Three

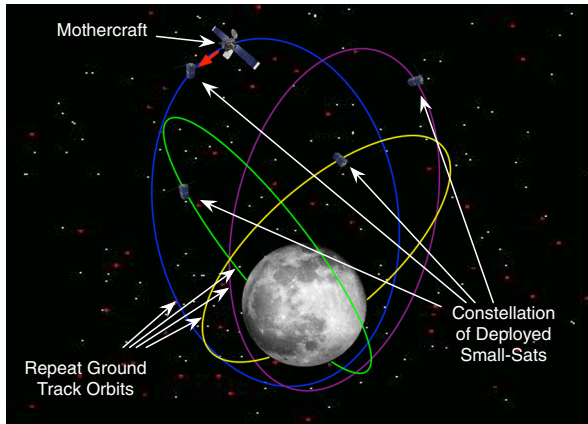


Fig. 1 Small satellites in a lunar flower constellation deployed by mothercraft

of the four small-sats have already been deployed into their orbits and the mothercraft has just deployed the final satellite.

This paper investigates a mission scenario where a mothercraft deploys a cluster of small-sats into a single petal of a flower constellation for a planar formation, and into a multi-petal configuration for a three-dimensional constellation. Of interest is how such constellations can be deployed without the small-sats performing fuel-expensive maneuvers, but rather letting the mothercraft do all repositioning. The small-sats are assumed to depart the mothercraft with a relative velocity typical for a cubesat deployment system. Finally, as flower constellations only consider J_2 -frozen orbits, and the lunar gravity field has other strong perturbations, station keeping maneuvers are developed and studied to maintain a flower constellation in the presence of these lunar perturbations.

Flower Constellations at the Moon

Flower constellations are an interesting family of constellations being studied extensively by Daniele Mortari at Texas A&M University. A full development of the flower constellation setup algorithm is found in References [6–8], and [9]. Flower constellations are characterized by their repeat groundtracks and their axis of symmetry. Flower constellations are at J_2 -frozen inclinations of either 63.4° or 116.6° and arguments of periapsis of either 90° or 270° . As these inclination angles are determined independent of the actual J_2 value, the J_2 -frozen inclinations are the same for the moon and the Earth. The remaining orbital parameters are selected based on matching the nodal period of the orbit with the nodal period of the central body about which the constellation is orbiting with some specified phasing. Scale factors for the number of days and the number of revolutions to repeat the groundtracks determine the period of repetition for the constellation [7]:

$$T_r = N_p T_\Omega = N_d T_{\Omega_B} \tag{1}$$

In Eq. 1, T_r is the period of repetition for the groundtracks, N_p is the number of revolutions to repeat, T_Ω is the nodal period of the orbit, N_d is the number of days to repeat, and T_{Ω_B} is the nodal period of the primary body. Another important parameter is the number of satellites, N_s . Flower constellations are named based on these three parameters as N_p - N_d - N_s constellations. The flower constellation period equation derived in Reference [6] is given in Eq. 2a. In Eq. 2b, ω_ζ is the angular rotation rate of the Moon, n is the mean motion, R_ζ is the equatorial radius of the Moon, p is the semi-latus rectum, and J_2 is the oblateness of the Moon. The classical set of orbital elements, $\mathbf{e} = (a, e, i, \Omega, \omega, M)$ are used.

$$T = \frac{2\pi}{\omega_\zeta} \frac{N_d}{N_p} \left(1 + 2\xi \frac{n}{\omega_\zeta} \cos i \right)^{-1} (1 + \xi \chi) \quad (2a)$$

$$\xi = \frac{3R_\zeta J_2}{4p^2} \quad (2b)$$

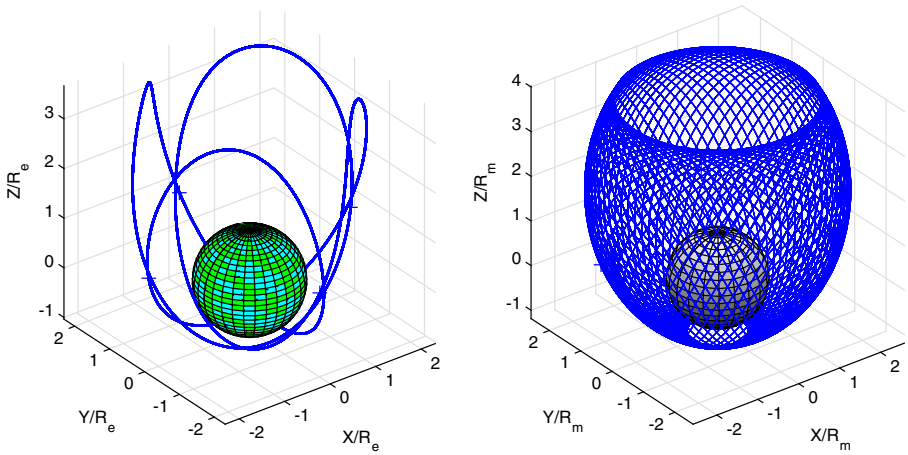
$$\chi = 4 + 2\sqrt{1 - e^2} - \left(5 + 3\sqrt{1 - e^2} \right) \quad (2c)$$

The anomalistic period is the periapsis-to-periapsis period and is given by the classic period equation as:

$$T = 2\pi \sqrt{\frac{a^3}{\mu}} \quad (3)$$

The expression in Eq. 2a can be equated to Eq. 3 and a numerical solver, such as MATLAB's built-in solver `vpasolve.m`, can be used to calculate a . From the semi-major axis, the eccentricity can be found, based on the design input for the radius of periapsis using the relationship $r_p = a(1 - e)$. It should be noted that the number of days to repeat (N_d) is defined as a day for the primary body. The Moon takes 27.32 Earth days to complete one rotation, so that an N_d of one lunar day corresponds to 27.32 Earth days. The long rotation period of the Moon creates very large orbits when $N_d = 1$, so that the perturbations from the Earth are dominant and the satellites actually escape Lunar orbit. A solution is to drastically increase the number of petals, N_p , to at least 50. A comparison of flower constellations at the Moon and Earth are shown in Fig. 2 in the body-fixed frame and in Fig. 3 in the inertial frame. The inertial orbits look very similar but the relative orbits as seen in the Earth and Moon body fixed frame are drastically different due to the rotation periods of the central bodies. The new look of flower constellations at the Moon creates so many petals that they become difficult to distinguish from one another. The term vase is perhaps now more appropriate to describe the look of the constellations in the relative frame.

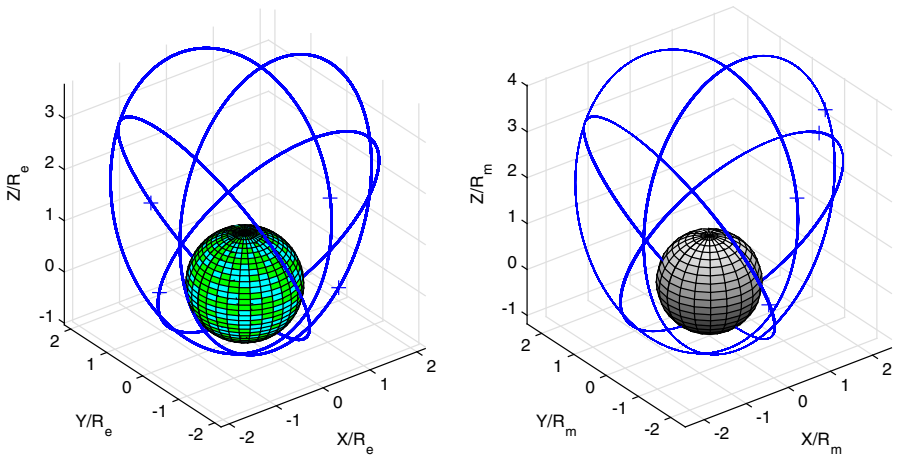
While the application of flower constellations to the Moon is novel, Russell and Lara in Reference [10] investigated long-lifetime repeat groundtrack orbits at the Moon. Periodic solutions where the normalized period of the orbit exactly matched one period of the Moon's revolution plus the additional change in the longitude of the ascending node of the orbit were desired [10]. This is in effect matching the nodal period of the orbit to the period of the Moon's rotation, as is achieved by flower constellations. The results of Reference [10] were merely families of solutions for frozen orbits where the number of orbit revolutions varied from 73 to 328 cycles, while the



(a) 4-1-4 Flower constellation at Earth (b) 73-1-4 Flower constellation at the Moon

Fig. 2 Flower constellation relative orbits at Earth and the Moon

revolution of the Moon was held to one. Interestingly, these orbits are simply flower constellations with 73 to 328 petals, so that they also appear as vase constellations in the relative frame. However, these solutions require a specific set of orbital elements, whereas in Mortari’s flower constellations, all the orbits have the same element set with the exception of the RAAN. In order to freeze orbits at the moon, the irregular perturbations from its gravity field and third-body effects from the Sun and Earth must be accounted for. This results in individual frozen orbit solutions that cannot



(a) 4-1-4 Flower constellation at Earth (b) 73-1-4 Flower constellation at the Moon

Fig. 3 Flower constellation inertial orbits at Earth and the Moon

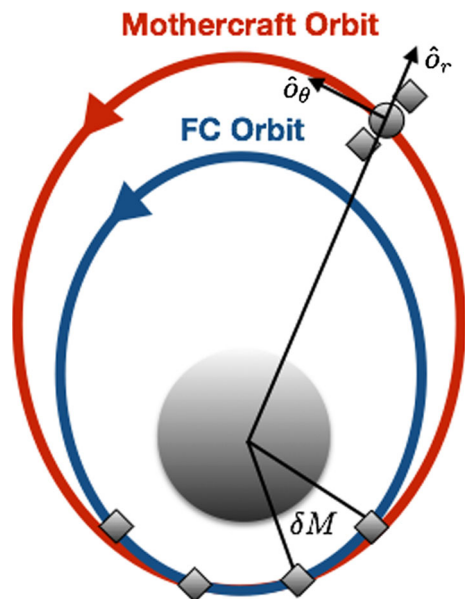
apply to the identical RAAN distributed orbits of a flower constellation. Therefore, for the purposes of this work, the J_2 -frozen orbit definition of flower constellations will still be used, with the understanding that J_2 is not the dominant perturbation at the moon. Therefore, station keeping maneuvers will be necessary to maintain the repeat groundtracks of the flower constellations in the presence of the perturbations at the moon.

Single Petal Deployment Scheme

Deployment is a primary challenge in the establishment of a constellation at the Moon. The mothercraft must do all the maneuvering and then deploy the small-sats into their desired orbits. A string-of-pearls formation within a flower constellation orbit can be created, and is relatively simple to deploy. This configuration is referred to as a single petal formation due to the nature of the single inertial orbit. The mothercraft deploys the satellites from an orbit that has a larger semimajor axis, and, therefore, longer period than the desired flower constellation orbit. A mean anomaly spacing of δM is desired between each flower constellation satellite. A factor, K , is used to determine how many orbits the mothercraft will complete between deploying sequential satellites. Equation 4 shows the relationship between the mothercraft period (T_{MC}) and the period of the flower constellation orbit (T_{FC}), where n_{FC} is the mean motion of the flower constellation orbit. This deployment scheme is shown in Fig. 4.

$$T_{MC} = T_{FC} + \frac{\delta M}{n_{FC}K} \quad (4)$$

Fig. 4 Single Petal Deployment Scheme



Through increasing K , the semimajor axis difference can be decreased, which decreases the relative velocity between the mothercraft and flower constellation orbits. Reducing this relative speed decreases the deployment speed required as the flower constellation satellites are released and put into their proper orbit slots. A small semimajor axis difference is desired as the impulsive change in velocity, ΔV , that matches the small satellites to the flower constellation orbits will be entirely achieved by the cubesat deployment system on the mothercraft. The poly picosatellite orbital deployer (P-POD) is a standard deployment system and will be used as a baseline for the attainable ΔV in the cubesat deployment. The nominal rates of deployment for the P-POD have been shown to be 1.6 – 2.0 m/s [11].

Once the mothercraft period has been determined, the semimajor axis can be solved for using the standard period expression given in Eq. 3. The radius of periapsis is set to the same radius of periapsis of the flower constellation orbit, which was a user input in the flower constellation design. From the radius of periapsis and semimajor axis of the mothercraft deployment orbit, the eccentricity may be found. The deployment is then implemented by releasing a satellite at every K^{th} periapsis passage of the mothercraft. The required ΔV at which the flower constellation cubesats must be released is determined by the difference in the mothercraft and flower constellation orbit velocities at periapsis. The well-known vis-viva equation is useful to solve for the velocity, v_p , at a periapsis radius, r_p , of both mothercraft orbit and the flower constellation orbit, as given in Eq. 5 [12]. The impulsive ΔV required is the difference between these two periapsis velocities. This process continues until all desired satellites have been deployed.

$$v_p = \sqrt{\frac{2\mu}{r_p} - \frac{\mu}{a}} \quad (5)$$

Single Petal Mothercraft Maneuver

After deployment is complete, the mothercraft must maneuver from the deployment orbit to the longterm communications orbit. The longterm communications orbit creates a relative orbit that is designed to orbit the flower constellation orbit element barycenter (FC barycenter). The orbit element barycenter is calculated by finding the average of the flower constellation satellite elements assuming that all flower constellation satellites are identical and have the same mass. The desired communications orbit for the mothercraft will have the same orbit elements as the FC barycenter but with an eccentricity difference. An eccentricity difference in formation flying creates a 2:1 ellipse of the mothercraft about the FC barycenter. This is a unique application of a flower constellation where a formation flying scheme is achieved, which could be strategic for specific science missions. The simple constellation geometry avoids the more complex out-of-plane maneuvers required of a multi-petal configuration. However, this configuration still allows for a distributed nature of the small satellites' sensor locations. At the end of deployment, the mothercraft will have a difference in a , e , and M from the FC barycenter. The semimajor axis and eccentricity differences are typically small, due to the factor K . However, the mean anomaly difference from

the barycenter at the end of deployment will be half of the prescribed string-of-pearls mean anomaly range, ΔM . A correction is performed to maneuver the mothercraft into the communications orbit. The first burn occurs at the first periapsis passage after the final flower constellation satellite deployment at periapsis. This maneuver places the mothercraft into a phase orbit that will correct the mean anomaly error by altering the semimajor axis (a), eccentricity (e), and radius of apoapsis (r_a) of the mothercraft. Based on the desired phase orbit, the semimajor axis, and the initial radius of periapsis (r_p), the radius of apoapsis and the eccentricity will change according to Eq. 6a.

$$r_p = a(1 - e) \quad (6a)$$

$$r_a = a(1 + e) \quad (6b)$$

It is recalled that in the final mothercraft orbit, only an eccentricity difference is desired from the flower constellation satellites. For an orbit to have the same semimajor axis as another orbit, but a different eccentricity, the radii of periapsis and apoapsis must both be shifted. The first burn will have already shifted the radius of apoapsis, which can contribute to an eccentricity difference in the final mothercraft orbit. Therefore, the second burn is desired to occur at apoapsis in order to maintain the shifted radius of apoapsis while still matching the desired semimajor axis by now shifting the radius of periapsis. Since the first burn occurs at periapsis and the second at apoapsis, the mean anomaly correction will occur over 1.5 phase orbits. In other words, $2/3$ of the mean anomaly error is corrected in one phase orbit period and the remaining $1/3$ is corrected in the final half-phase orbit period. The phase orbit is designed so that the mothercraft periapsis is raised to an orbit that has a period equal to the flower constellation orbit period, plus the time needed to cover $2/3$ of the mean anomaly difference. This is described by Eq. 7, where ϕ is the phase angle between the mothercraft and the FC barycenter. In other words, ϕ is the initial mean anomaly error ($\Delta M/2$). In this study, ϕ is a negative value (desired minus actual), and the phase orbit will have a smaller semimajor axis, and therefore, shorter period, than the flower constellation orbit.

$$T_{\text{phase}} = \frac{2\pi + \frac{2\phi}{3}}{n_{\text{FC}}} \quad (7)$$

From Eqs. 4 and 7, the phase orbit semimajor axis can be determined. From there, Eq. 5 can be used to find the velocity of the mothercraft at periapsis in the original deployment orbit ($V_{p,\text{deploy}}$) and the velocity at periapsis required for the phasing orbit ($V_{p,\text{phase}}$). The difference in these velocity magnitudes is the impulsive ΔV_1

Table 1 Orbital elements for single petal flower constellation satellites

Satellite	a (km)	e	i (deg)	ω (deg)	Ω (deg)	M_0 (deg)
1, 2, 3, 4	5053.73	0.60670	63.4	270	0	0, 7, 14, 21

required to place the mothercraft into the phasing orbit, with the burn applied in the along-track direction.

$$a_{\text{phase}} = \left[\mu \left(\frac{6\pi + 2\phi}{6\pi n_{\text{FC}}} \right)^2 \right]^{1/3} \tag{8a}$$

$$V_{\text{p,deploy}} = \sqrt{\frac{2\mu}{r_{\text{p,deploy}}} - \frac{\mu}{a_{\text{deploy}}}} \tag{8b}$$

$$V_{\text{p,phase}} = \sqrt{\frac{2\mu}{r_{\text{p,deploy}}} - \frac{\mu}{a_{\text{phase}}}} \tag{8c}$$

$$\Delta V_1 = V_{\text{p,phase}} - V_{\text{p,deploy}} \tag{8d}$$

After 1.5 phasing orbits the mothercraft makes a second burn at apoapsis (ΔV_2) to match the desired flower constellation semimajor axis. Again, the magnitude of this burn is found using the radius of apoapsis of the phase orbit and the semimajor axis of the phase orbit and the desired orbit to find the initial and final velocities at apoapsis respectively. This burn is also in the along-track direction; once completed, the mothercraft will be in the desired longterm orbit with only an eccentricity difference from the flower constellation barycenter.

The flower constellation to be studied for the numerical simulation is a 73-1-4 constellation with a periapsis height of 250 km. A mean anomaly range (ΔM) of 21° is specified, resulting in the orbital elements given in Table 1. A value of $K = 5$ in Eq. 4 is selected resulting in a required ΔV magnitude of 0.55 m/s, which is well within the capability of a cubesat deployer. The deployment simulation does not include any perturbations. It is important to note that in real applications, the irregular gravity field of the Moon and third-body effects from the Sun and Earth would need to be considered. Instead, this simulation assumes that any initial errors that would result from ignoring perturbations can be corrected for through the controls in the first longterm orbit maintenance maneuver.

The mean anomalies achieved at the end of the deployment phase for the constellation satellites are shown in Table 2. In comparison to the mean anomalies in Table 1, it can be seen that the desired values are achieved with small errors. These errors can be corrected for in the first longterm orbit maintenance maneuver.

The inertial orbits at the end of the deployment phase are shown in Fig. 5. The red orbit is the orbit of the mothercraft and the blue orbit is the flower constellation orbit. In this view, the two orbits appear to be the same, but there are small differences in semimajor axis and eccentricity, as shown in Table 3. The red circle indicates the mothercraft’s location at the final deployment and the blue plus signs represent the

Table 2 Mean anomalies achieved for flower constellation satellites after deployment

Satellite	1	2	3	4
Mean anomaly (deg)	-0.4275	6.5722	13.5725	20.5729

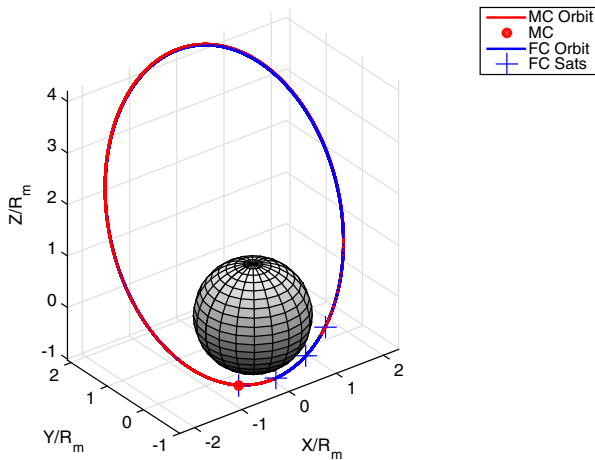


Fig. 5 Inertial Orbits at moment of final FC satellite deployment

flower constellation satellites. The final flower constellation and mothercraft satellites are shown to be at the same location at the moment of deployment.

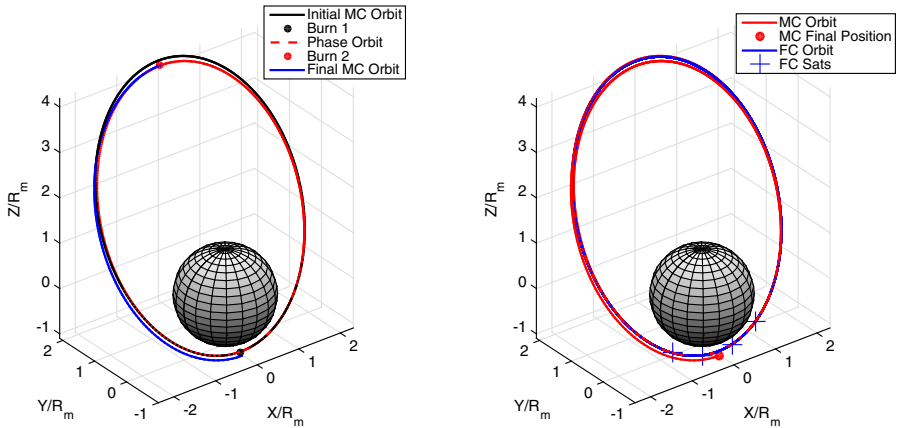
Now that deployment of the flower constellations satellites is complete, the mothercraft must move into its longterm communications orbit. At the end of the deployment phase, the initial mean anomaly error is -11.90° . The inertial orbits during the mean anomaly correction period are shown in Fig. 6. The first burn has a magnitude of 4.2794 m/s and the second burn has a magnitude of 14.4396 m/s, both in the along-track direction. These burn magnitudes are small and found to be acceptable.

In Fig. 6a, the mothercraft starts at periapsis on the black orbit. The black dot shows where the first maneuver is made at periapsis to lower the mothercraft into the phase orbit shown in red. The phase orbit elements are given in Table 4. After 1.5 phase orbits, the second maneuver is made at apoapsis, marked by the red dot. The resulting orbit is the final mothercraft orbit shown in blue in Fig. 6a. This new mothercraft orbit is also given in Table 5 and matches the FC barycenter orbit but with an eccentricity difference. The mothercraft orbits during this correction period are shown with the flower constellation orbit in Fig. 6b. The final position of the mothercraft relative to the flower constellation satellites can be seen; as desired, the mothercraft is aligned with the mean anomaly of the FC barycenter.

The initial and final flower constellation and mothercraft orbit elements, as well as the phase orbit elements are given in Table 5. All values in Table 5 are taken at

Table 3 FC and mothercraft orbits during deployment

Orbit	a (km)	e	i (deg)	ω (deg)	Ω (deg)
Flower constellation	5053.73	0.60670	63.4	270.0	0
Mothercraft	5066.82	0.60771	63.40	270.0	0



(a) Mothercraft Mean Anomaly Phase Orbit (b) Inertial Orbits at end of mean anomaly correction

Fig. 6 Mothercraft mean anomaly correction

the FC barycenter apoapsis passage, as this is where the final maneuver occurs. An eccentricity difference between the final FC barycenter and final MC orbits are all that remain.

Multi-Petal Deployment Scheme

In contrast to the single petal formation, the full flower constellation involving multiple orbit planes will be referred to as a multi-petal constellation, due to the multiple inertial orbits. This deployment scheme is more complicated as it does involve large plane changes in the RAAN. One-burn plane changes are the simplest maneuver to alter the plane of an orbit and will serve as the baseline cost. A one-impulse plane change must be performed at one of the two nodes where the initial and desired orbit planes intersect. This optimal point is found numerically after looping through various values of the mean anomaly in two neighboring flower constellation orbits. Two node possibilities exist; the node located at the larger radius magnitude will be less costly as the local velocity will be lower. Two neighboring orbits from a 73-1-4 flower constellation are shown in Fig. 7 with the two nodes for one-impulse maneuvers shown by the red dots. The cost of this one-burn plane change can be found by calculating the magnitude of the difference in the inertial velocity vectors between the two orbits at the node.

Table 4 Phase orbit elements

	a (km)	e	i (deg)	ω (deg)	Ω (deg)
Phase Orbit	4979.21	0.60081	63.40	270.00	0

Table 5 Orbits during mean anomaly correction

Orbit	a (km)	e	i (deg)	ω (deg)	Ω (deg)	M (deg)
Initial FC barycenter	5053.73	0.60670	63.40	270.00	0	11.8754
Initial MC	5066.82	0.60772	63.40	270.00	0	360.9996
Final FC barycenter	5053.73	0.60670	63.40	270.00	0	359.8478
Final MC	5053.73	0.57721	63.40	269.98	359.80	359.8455

It is known, however, that three-impulse plane change maneuvers (i.e. bi-elliptic) are usually optimal over one-impulse plane changes [13]. A bi-elliptic plane change is shown in Fig. 8, where the majority of the plane change occurs at the second maneuver, and a small amount occurs at the first and third burns. Unfortunately, a bi-elliptic maneuver can be problematic at the Moon, where the Sun and Earth can cause significant perturbations in the large transfer orbits. A modified bi-elliptic plane change with only a slight increase in the semimajor axis is investigated. It is assumed that the mothercraft is initially in one of the desired flower constellation orbits, and has already deployed the first small-sat. In the deployment of the remaining $N_s - 1$ satellites it is assumed that the mothercraft performs all burns to conserve fuel in the small-sats.

The optimal orbits can be found using MATLAB's built-in constrained optimizer, `fmincon.m`. A transfer orbit sequence will be considered optimal if it is less costly than an impulsive maneuver. The goal of this optimization problem is to find the optimal values of the parameters given in Table 6.

Intuitively, it is expected that M_1 will be near periapsis and that the first burn, ΔV_1 , will raise the apoapsis of the orbit. Some of the plane change will be accomplished by ΔV_1 and ΔV_3 , but both of these maneuvers will primarily be responsible for adjusting the size (semimajor axis) and shape (eccentricity) of the orbits. The

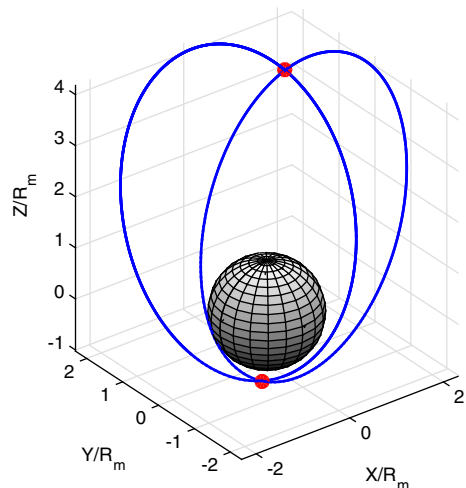
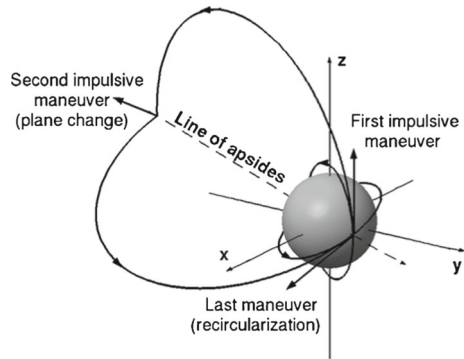
Fig. 7 Nodes for one-impulse maneuvers

Fig. 8 Bi-elliptic three-burn plane change [13]



majority of the plane change will occur with ΔV_2 , with this burn doing very little to change either the size or shape of the transfer orbit. The third burn, ΔV_3 is also expected to occur near periapsis as this maneuver will lower the orbit back to the flower constellation semimajor axis and eccentricity values.

Scaling is very critical in optimization. All parameters to be optimized—as well as bounds and constraints on the system—must all be the same order of magnitude. For this problem, all values are desired to be between ± 1 . In order to achieve this scaling, normalization is used for parameters that would otherwise fall outside of the ± 1 scale limits. The mean anomaly is normalized by 2π with a lower bound of 0 and an upper bound of 1. The ΔV components do not require normalizing as they are already bounded to be between ± 0.5 km/s.

The cost function for this problem is simply the total ΔV required for the three-burn maneuver. As such, the cost is given by the sum of the magnitudes of the individual burns. The first and second burn ΔV components are parameters to be optimized. The third burn ΔV_3 is simply determined by the magnitude of the difference between the velocity vector at M_2 in the final flower constellation orbit and the velocity vector at the end of the second transfer orbit. The cost function is given by Eq. 9.

$$f = \Delta V_1 + \Delta V_2 + \Delta V_3 \tag{9}$$

There are also some constraints on this problem in addition to the bounds that were placed on the optimization parameters. These constraints take the form of either equality constraints or inequality constraints. The equality constraints state that the components of the inertial position vectors at the end of the second transfer orbit must

Table 6 Optimization parameters

M_1	Mean anomaly in initial FC orbit at which to perform first impulsive burn
ΔV_1	Inertial delta-V vector for first impulsive burn
M_T	Mean anomaly in transfer orbit at which to perform second impulsive burn
ΔV_2	Inertial delta-V vector for second impulsive burn
M_2	Mean anomaly in final FC orbit at which to perform third impulsive burn
ΔV_3	Inertial delta-V vector for third impulsive burn

match the components of the position vector at M_2 in the final flower constellation orbit. The position vectors (\mathbf{R}) are normalized by the semimajor axis of the flower constellation orbits for scaling purposes, as given by Eq. 10

$$\mathbf{g} = \frac{\mathbf{R}_{T2f}}{a_{FC}} - \frac{\mathbf{R}_{FC2M_2}}{a_{FC}} = \mathbf{0} \tag{10}$$

There are several inequality constraints on the problem. The first constraint is that the eccentricities of the transfer orbits must be less than one to ensure an elliptic transfer orbit. The second constraint is that the radius of periapsis of the transfer orbits must be larger than the radius of the Moon (R_m) in order to prevent impact. This constraint uses the radius of the Moon to normalize for proper scaling. The final inequality constraint is that the semimajor axis of the transfer orbits must be less than a specified semimajor axis limit. This constraint is normalized by the semimajor axis of the individual transfer orbits to ensure proper scaling. The inequality constraints are summarized by Eq. 11a

$$h_1 = e_{T1} - 1 \leq 0 \tag{11a}$$

$$h_2 = e_{T2} - 1 \leq 0 \tag{11b}$$

$$h_3 = \frac{R_m - r_{p,T1}}{R_m} \leq 0 \tag{11c}$$

$$h_4 = \frac{R_m - r_{p,T2}}{R_m} \leq 0 \tag{11d}$$

$$h_5 = \frac{a_{T1} - a_{max}}{a_{T1}} \leq 0 \tag{11e}$$

$$h_6 = \frac{a_{T2} - a_{max}}{a_{T2}} \leq 0 \tag{11f}$$

Within the confines of the small bi-elliptic strategy employed in this study, there exist trade-offs between the fuel spent in the first burn to raise apoapsis and fuel savings in changing the RAAN at a larger radius of apoapsis where the velocity is smaller. Additionally, large orbits about the Moon are greatly impacted by third-body perturbations from the Sun and Earth. The limit given to the semimajor axis of the transfer orbits, a_{max} , will greatly impact the solution. The larger a_{max} is, the lower the overall cost, since the largest burn, ΔV_3 will decrease. However, it is desired for the transfer orbits to remain relatively small in order to avoid significant third-body perturbations. Perturbations are not included in this optimization, with the assumption that small errors that would accumulate over the transfer duration can be corrected for either by the mothercraft once in the final orbit, or by the children craft after deployment in the orbit maintenance maneuvers.

Table 7 Orbital elements for 73-1-4 multi-petal flower constellation satellites

Satellite	a (km)	e	i (deg)	ω (deg)	Ω (deg)	M_0 (deg)
1, 2, 3, 4	5053.73	0.60670	63.4	270	0, 270, 180, 90	0, 180, 0, 180

Table 8 Final values of optimization parameters for $a_{\max} = 9000$ km

M_1 (deg)	ΔV_{1x} (km/s)	ΔV_{1y} (km/s)	ΔV_{1z} (km/s)	M_T (deg)	ΔV_{2x} (km/s)	ΔV_{2y} (km/s)	ΔV_{2z} (km/s)	M_2 (deg)
338.3	0.0478	-0.0557	-0.1172	154.3	0.1716	0.1827	-0.2772	40.97

The flower constellation to be studied for the numerical simulation is a 73-1-4 constellation with a height of periapsis of 250 km. The orbital elements for the satellites in this constellation are summarized in Table 7.

The baseline cost of a one-burn RAAN change is calculated and found to be 0.93084 km/s. For a small bi-elliptic method to be optimal over the one burn strategy, it must have a total cost less than 0.93084 km/s. Initially, the limit on the transfer orbit semimajor axis is set to 9000 km. The total cost for this maneuver is found to be 0.686234 km/s and is, therefore, optimal over the one-burn maneuver with a cost savings of 0.24460 km/s. The final values for the optimization parameters are summarized in Table 8.

The trajectories for this optimal three-burn maneuver are shown in Fig. 9. The first burn at M_1 is marked by the turquoise asterisk, the second burn at M_T by the light blue asterisk, and the third burn at M_2 with the magenta asterisk. While not a constraint on the problem, the first and second transfer orbits have nearly matching orbital elements with the exception of RAAN and inclination, as these were desired to be changed in the maneuver. The orbital elements of the transfer orbits are summarized in Table 9.

Ultimately, the limit placed on the semimajor axis of the transfer orbits significantly alters the optimal solution that can be found. As the semimajor axis limit becomes smaller, the bi-elliptic nature of the transfer orbits no longer holds since the transfer orbit is not allowed to be much larger than the flower constellation orbits

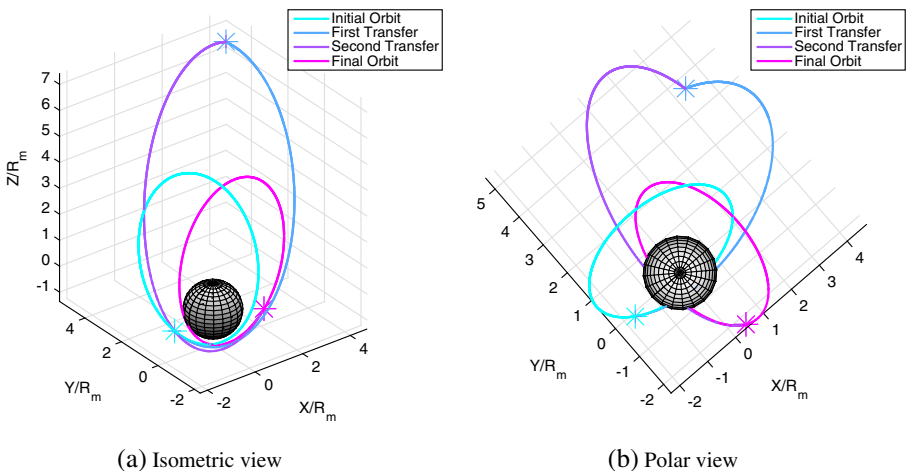


Fig. 9 Optimal three-burn orbits for $a_{\max} = 9000$ km

Table 9 Orbital elements for transfer orbits for $a_{\max} = 9000$ km

Transfer orbit	a (km)	e	i (deg)	ω (deg)	Ω (deg)	M_0 (deg)
1	8985.24	0.75436	63.50	253.38	0.01	352.45
2	8994.71	0.72790	65.16	293.49	270.89	182.38

themselves. This change occurs approximately at a semimajor axis limit of 5200 km. However, even in these schemes, a three-burn maneuver is still shown to be optimal over a one-burn maneuver. Again, the baseline cost is 0.93084 km/s. When the limit on the transfer orbits semimajor axis is set to 5200 km the total cost for the three-burn maneuver is found to be 0.86228 km/s and is, therefore, optimal over the one-burn maneuver with a cost savings of 0.06855 km/s. The final values for the optimization parameters are summarized in Table 10.

While still optimal over the one burn maneuver, the strict semimajor axis limit causes the transfer orbits to take on a new form, as shown in Fig. 10 and summarized in Table 11. The first burn is performed near apoapsis instead of closer to periapsis in Fig. 9. The apoapsis of the first transfer orbit is only slightly raised to a semimajor axis of 5198.66 km and almost a full orbit is completed before the second maneuver. After the second burn, the orbit elements almost match the desired final constellation orbit, with the third burn eliminating these small differences.

These simulations have assumed a 73-1-4 constellation, so that there are four orbit planes, each at a 90° RAAN separation. However, as N_s is increased, the $\Delta\Omega$ between orbits decreases. It is desired to know if the three-burn method is always optimal over the one-burn method. For a semimajor axis limits of 9000 and 5200 km, the parameter N_s is varied from four to twenty and the cost of the three-burn maneuver is compared to a one-burn maneuver. The results are plotted in Fig. 11. The values of $\Delta\Omega$ corresponding to N_s are also plotted.

It can be seen in Fig. 11a, that the initial difference between the one-burn and three-burn maneuver for $a_{\max} = 9000$ km is greater than in Fig. 11b for $a_{\max} = 5200$ km. Regardless of the semimajor axis limit, as the number of satellites is increased, the RAAN change required per satellite decreases and the cost of the three-burn maneuver approaches the cost of the one-burn maneuver. However, the three-burn maneuver is always less than or equal to the one-burn method.

It was also desired to observe trends in the cost for the establishment of the entire constellation as N_s is varied. For the semimajor axis limit of 9000 km, the general

Table 10 Final values of optimization parameters for $a_{\max} = 5200$ km

M_1 (deg)	ΔV_{1x} (km/s)	ΔV_{1y} (km/s)	ΔV_{1z} (km/s)	M_T (deg)	ΔV_{2x} (km/s)	ΔV_{2y} (km/s)	ΔV_{2z} (km/s)	M_2 (deg)
158.3	0.0675	0.1525	-0.3769	141.3	0.1784	0.0887	-0.3987	25.34

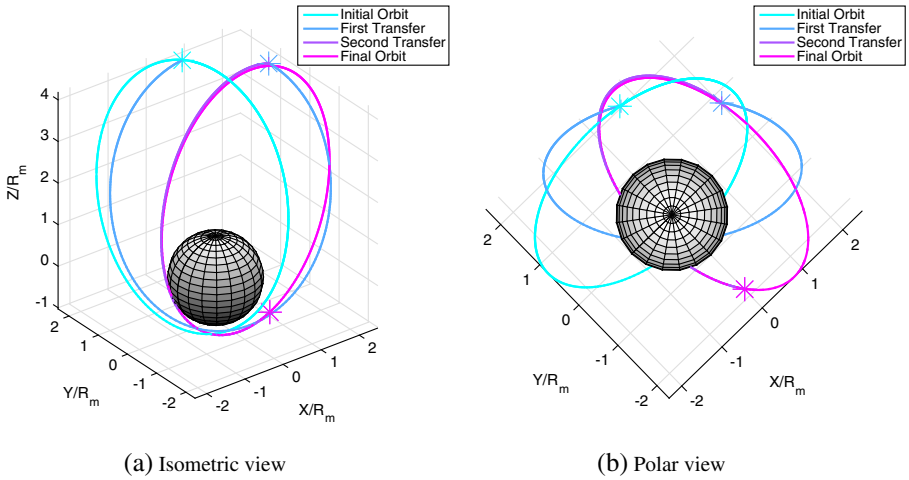


Fig. 10 Optimal three-burn orbits for $a_{\max} = 5200$ km

trend is that the total cost grows as the number of satellites increases, due to the increased number of maneuvers. However, there are some interesting fluctuations in the total cost for eight, nine, and eleven satellites. It is actually less expensive to establish an eight or nine satellite constellation than one with only seven satellites. Likewise, it costs less to create an eleven satellite constellation compared to a ten satellite constellation. For the semi-major axis limit of 5200 km, the general trend of increasing total cost is more consistent than for the semimajor axis limit of 9000 km. The only deviants from the trend are a ten satellite constellation, which is equal in cost to a nine satellite constellation, as well as a twelve satellite constellation, which is equal in cost to an eleven satellite constellation.

Ultimately, for any number of satellites, N_s , a three-burn maneuver should be used to deploy the individual satellites in the constellation. The larger the semimajor axis limit, the less costly the three-burn maneuver. However, the larger the transfer orbits, the more prominent the third-body perturbations will be, perhaps requiring larger initial corrections by the flower constellation satellites after deployment. As is true in all optimization problems, the optimal solution is dependent upon the requirements of the problem at hand.

Table 11 Orbital elements for transfer orbits for $a_{\max} = 5200$ km

Transfer orbit	a (km)	e	i (deg)	ω (deg)	Ω (deg)	M_0 (deg)
1	5198.66	0.60928	65.27	268.93	317.96	222.03
2	5101.79	0.60818	63.43	270.67	269.99	205.59

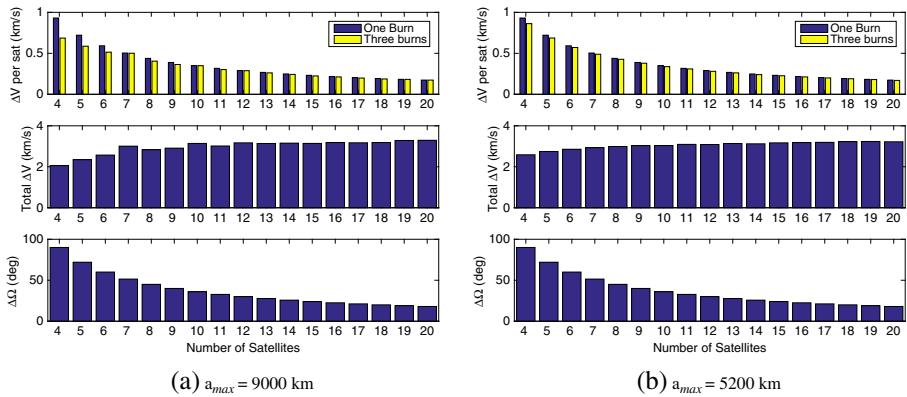


Fig. 11 Maneuver costs for various values of N_s

Multi-Petal Mothercraft Maneuver

Once the flower constellation has been fully deployed, the mothercraft must maneuver to a longterm communications orbit. The requirement of this orbit are that the mothercraft must periodically pass by all of the children craft in order to communicate with them and relay back to the Earth due to the limited communications range of the small-sats. A polar orbit for the mothercraft has been selected as it maintains the same symmetry as the flower constellation about the spin axis of the Moon. The semimajor axis is desired to be larger than the flower constellation orbit semi-major axis so that there is a period difference. This period difference will allow the mothercraft to travel by all children satellites rather than maintaining the same relative positions to the children satellites were the semimajor axis to match. The RAAN will drift with time due to lunar perturbations and this motion will not be controlled against, so that the initial RAAN is not a critical parameter. Therefore, to minimize fuel costs in this maneuver, the RAAN will not be changed from the final flower constellation orbit to the longterm mothercraft orbit.

Once again, a 73-1-4 flower constellation is studied. The desired semimajor axis for the longterm mothercraft orbit is chosen to be 10 % larger than the flower constellation semimajor axis. As it will be shown later, it is the inclination change from the J2 frozen inclination of 63.4° to a polar inclination of 90° that drives the cost of this maneuver. Therefore, the semimajor axis difference used is almost arbitrary. The initial mothercraft orbit elements are the same as the final flower constellation orbit. The desired elements are the same except for the polar inclination and semimajor axis. The initial and final elements for the mothercraft are summarized in Table 12.

The simplest way to move the mothercraft into the desired orbit is to first perform one orbit with small burns in the along-track direction at both periapsis and apoapsis to raise the semimajor axis of the orbit. The costs of these burns are found using the impulsive orbit element control equations of Reference [14]. Once the desired semimajor axis is obtained, the plane change maneuver can be performed. It is desired to perform this maneuver second as the velocity will be smaller in the larger orbit,

Table 12 Initial and final mothercraft orbits

Orbit	a (km)	e	i (deg)	ω (deg)	Ω (deg)
Initial orbit	5053.72	0.60670	63.4	270	90
Final orbit	5559.10	0.60670	90	270	90

decreasing the cost of the maneuver. The location at which to perform the plane change maneuver will be governed by the critical angle, θ_c at which plane change maneuvers are optimal. This burn will occur in the out of plane direction and is computed using the equation for ΔV_h in Reference [14]. The total baseline cost for this sequence of maneuvers was found to be 0.61438 km/s.

Similarly to the deployment scheme discussed for establishing the flower constellation orbits, this maneuver also involves a costly large plane change. Therefore, it is likely that there is a three-burn transfer orbit maneuver to change both the inclination and semimajor axis that would be optimal over the series of impulsive burns just discussed. The cost functions and constraints remain unchanged from Eqs. 9, 10, and 11a. The only difference between these two optimization problems is the initial and final orbits desired. It should also be noted that the impulsive burns for the baseline cost are all in the local vertical local horizontal (LVLH) frame whereas the burns to be optimized in the three burn transfer orbit scheme are inertial velocities. However, when comparing magnitudes, the frames used are irrelevant.

For the three-burn transfer orbit method to be optimal over the impulsive burn series strategy, it must have a total cost less than the baseline cost of 0.61438 km/s. The limit on the transfer orbits semimajor axis is set to 9000 km. The total cost for this maneuver is found to be 0.44432 km/s and is, therefore, optimal over the impulsive burn series with a cost savings of 0.17007 km/s. The final values for the optimization parameters are summarized in Table 13 and shown in Fig. 12.

The orbital elements of the transfer orbits are summarized in Table 14. Figure 12 shows that the second transfer orbit nearly matches the desired orbit. This is verified by comparing the orbital elements in Table 12 for the desired orbit to the elements in Table 14 for transfer orbit two. The final burn is a small burn that simply matches the two orbits more precisely.

Many orbits are feasible for the mothercraft longterm communications orbit, as long as the mothercraft periodically comes into communications range of all satellites in the constellation. The one example presented in this section is a good candidate orbit. The three-burn transfer orbit strategy used for this orbit can also be applied to other mothercraft maneuvers that may require large plane changes.

Table 13 Final values of optimization parameters for final mothercraft maneuver

M_1 (deg)	ΔV_{1x} (km/s)	ΔV_{1y} (km/s)	ΔV_{1z} (km/s)	M_T (deg)	ΔV_{2x} (km/s)	ΔV_{2y} (km/s)	ΔV_{2z} (km/s)	M_2 (deg)
60.09	0.1886	0.0200	0.1041	301.89	-0.2230	-0.0208	-0.0424	25.02

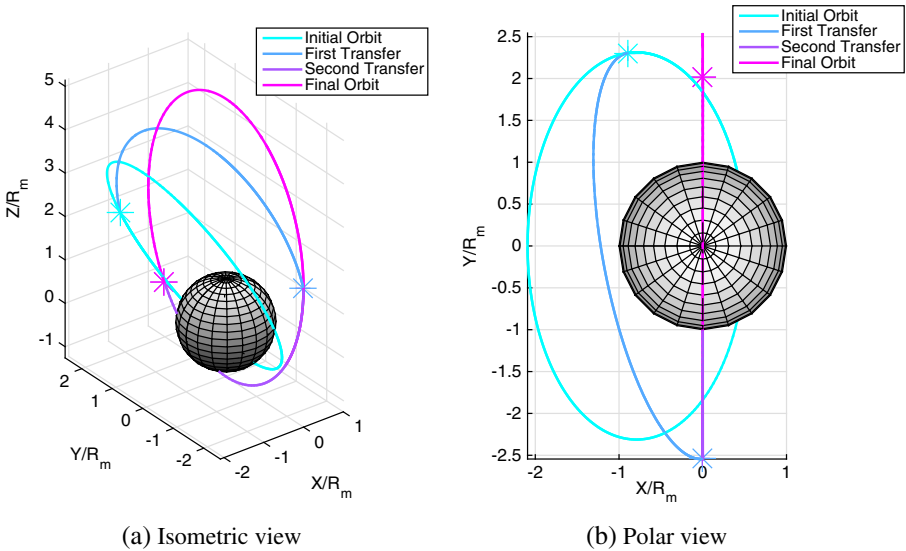


Fig. 12 Optimal three-burn orbits for $a_{\max} = 9000$ km

Longterm Maintenance

Once deployment is complete, the flower constellation satellites are subject to lunar perturbations. The orbits are not high-fidelity solutions and are only J_2 compatible, therefore, they must be corrected periodically to maintain the repeat groundtrack nature of the flower constellation. This will be simulated through propagating the orbits under the influence of the 50×50 lunar gravity field, as well as point mass effects from the Earth and Sun. The impulsive feedback control law developed in Reference [14] will be used to perform impulsive orbit element corrections in the simulation. The accumulated ΔV corrections from the impulsive control will be used to predict fuel expenditure, and from that, the constellation lifetime. As the lifetime maintenance is very similar for the single petal and multi-petal configurations, only the simulation for the multi-petal configuration is presented.

The relative orbits for the repetition period are shown in Fig. 13a. The overall vase shape is maintained, although the perfect latticework of the relative orbits is compromised by the lunar perturbations and the drift that occurs between control periods. The difference between the constellation with full perturbations and only J_2 can be seen by comparing Fig. 13b with Fig. 2b. However, the lunar surface coverage of the

Table 14 Orbital elements for transfer orbits for $a_{\max} = 9000$ km

Transfer Orbit	a (km)	e	i (deg)	ω (deg)	Ω (deg)	M_0 (deg)
1	5390.58	0.60714	76.04	271.01	100.87	53.66
2	5559.42	0.60663	90.00	270.00	89.94	304.78

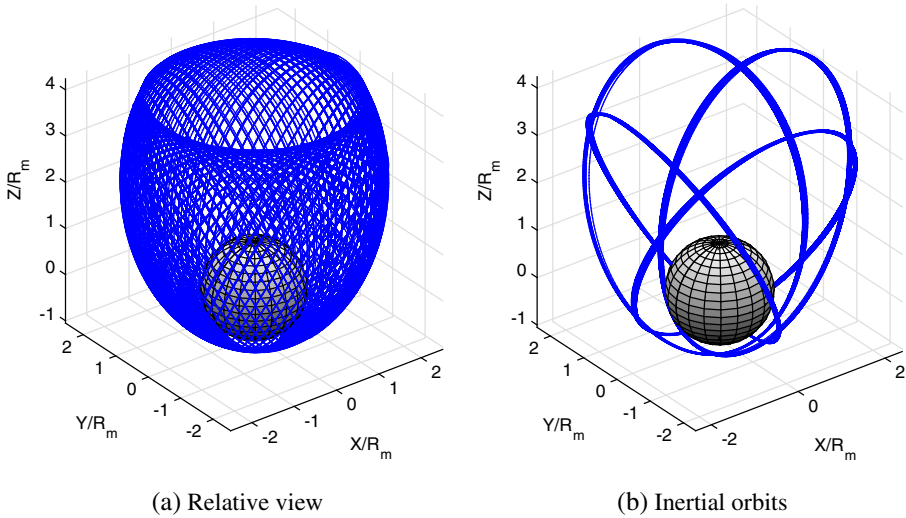


Fig. 13 73-1-4 multi-petal FC perturbed orbits

constellation is still achieved, just without the exact repeat groundtrack nature that would occur with only J_2 , or if controls were to be applied every orbit to constantly eliminate drift.

The inertial orbits over the repetition period are shown in Fig. 13b. It can be seen that the perturbations cause precession in the inertial orbits over the 27-day repetition period, by comparing Fig. 13b to Fig. 3b where only J_2 was included. The total control costs are sensitive to how close the corrections are applied relative to the desired locations of periapsis, apoapsis, and θ_c . It was found that satellite one experienced the largest ΔV and after further investigation, it was found to be due to how close the in-plane corrections were performed relative to the actual periapsis crossing. This is an implementation challenge and is manifested in the higher control ΔV cost for satellite one compared to the remaining satellites, as shown in Table 15. Since satellite one is the worst case, only the results of the control simulation for satellite one ($\Omega = 0^\circ$) are presented in detail.

The errors in the orbital elements for satellite one are shown in Fig. 14. From Fig. 14a, it can be seen that on average, a , e , and i do not grow, but rather osculate around a mean value. However, in Fig. 14b, ω , Ω , and M grow over the first five days before the first control cycle is implemented. However, after each control period,

Table 15 Total ΔV magnitude over five control orbits

Satellite	1	2	3	4
ΔV (m/s)	360.6	219.3	201.5	231.8

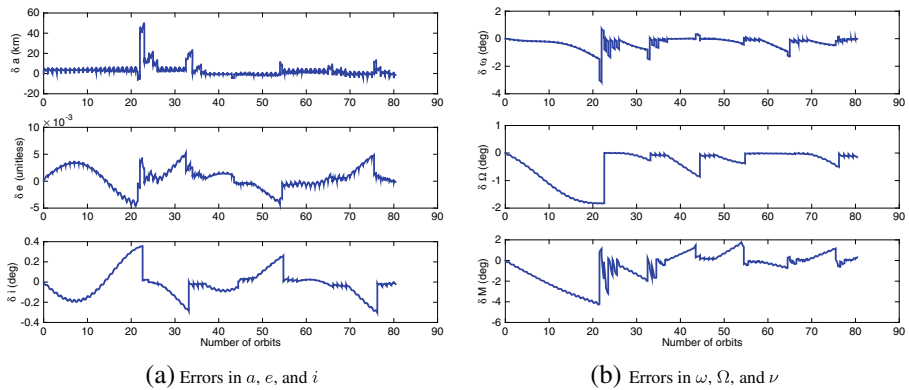


Fig. 14 Satellite one element errors controlling every four days

the element errors are reduced to nearly zero. In other words, the control sequence corrects the actual orbit elements to match the desired orbit elements. This behavior is better shown in Fig. 15: the red dashed line shows the desired elements and the solid blue line is the actual elements over time. After each sequence of five control orbits, the actual elements converge on the desired element values. In Fig. 15a, the desired values for a , e , i , and ω are all constant, as described in Table 7. However, the RAAN (Ω) is drifting over time. The control phase captures the drift behavior and converges to the current RAAN value rather than the initial RAAN, as shown in Fig. 15b. The initial jumps that occur at the beginning of each control phase for the in-plane elements (a , e , and ω) are all due to the application of the controls at a point near periapsis, but not exactly at periapsis. These errors that are introduced are eliminated in subsequent control orbits from the burns at apoapsis, where better accuracy is achieved due to the slower orbital velocity near apoapsis.

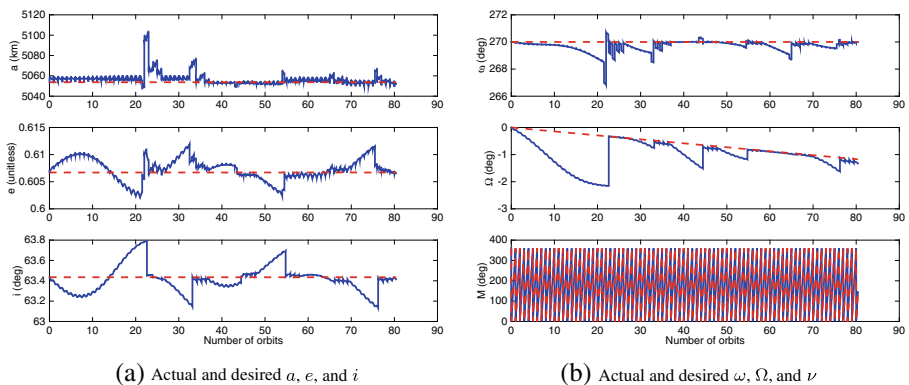


Fig. 15 Satellite one actual (solid) and desired (dashed) elements controlling every four days

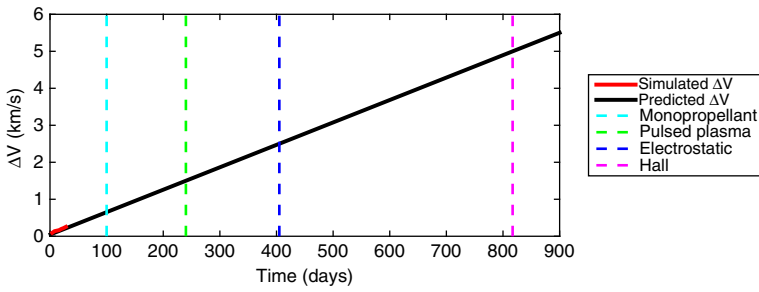


Fig. 16 Multi-petal FC lifetime prediction for a 4 kg satellite with 1 kg fuel

In order to predict the lifetime of a flower constellation at the Moon, two pieces of information are needed: the fuel required and the fuel available for each satellite. The ΔV required per 27-day repetition period, per satellite was given in Table 15 and corresponds to the fuel required. Two primary factors that affect cubesat fuel consumption are overall mass and the type of engine or propellant used. Reference [15] provides propellant mass required as a function of ΔV for various types of propellant assuming a 4 kg cubesat. This relationship is used to estimate the constellation lifetime.

In Fig. 16, the red curve in the bottom left of the plot is the actual calculated average ΔV s after every four days for 28 days. The black curve is the linear curve fit produced from the first 28 days of calculated burns, extrapolated for 900 days. It can be seen in Fig. 16 that for a monopropellant thruster and 1 kg of fuel, the constellation can last exactly 100 days. As the thruster efficiency increases in the form of a higher I_{sp} , the lifetime increases. A pulsed plasma thruster can support the constellation for 240 days, the electrostatic thruster extends the lifetime to just over 400 days, and the hall thruster provides the longest constellation lifetime at over 800 days.

Conclusion and Future Work

This work provided an initial investigation of the feasibility for establishing a flower constellation at the Moon. This constellation can take the form of either a single-petal constellation or a multi-petal constellation. Both constellations studied were 73-1-4 constellations with a height of periapsis of 250 km. The challenges of applying flower constellations to the Moon, optimal deployment schemes, and constellation lifetime and maintenance were all investigated. Overall, it has been demonstrated that flower constellations are indeed feasible at the Moon. In fact, the constellation can achieve a significant scientific mission with a lifetime of at least 90 days. While this investigation made many specific assumptions in the studies and simulations performed, the techniques can be generalized to any sort of constellation at any Moon or other celestial body, including orbits at Earth. The perturbations and constellation configuration would differ based on the central body involved.

References

1. Board, S.S., et al.: Assessment of impediments to interagency collaboration on space and earth science missions (2011)
2. Zuber, M.T., Smith, D.E., Watkins, M.M., Asmar, S.W., Konopliv, A.S., Lemoine, F.G., Melosh, H.J., Neumann, G.A., Phillips, R.J., Solomon, S.C., et al.: Gravity field of the moon from the gravity recovery and interior laboratory (GRAIL) mission. *Science* **339**(6120), 668–671 (2013)
3. The Kaguya project team, Kato, M., Sasaki, S., Takizawa, Y.: The kaguya mission overview. *Space Sci. Rev.* **154**, 3–19 (2010). doi:[10.1007/s11214-010-9678-3](https://doi.org/10.1007/s11214-010-9678-3)
4. Boshuizen, C., Mason, J., Klupar, P., Spanhake, S.: Results from the planet labs flock constellation (2014)
5. Gill, E., Sundaramoorthy, P., Bouwmeester, J., Zandbergen, B., Reinhard, R.: Formation flying within a constellation of nano-satellites: The QB50 mission. *Acta Astron.* **82**, 110–117 (2013). doi:[10.1016/j.actaastro.2012.04.029](https://doi.org/10.1016/j.actaastro.2012.04.029)
6. Wilkins, M.P., Bruccoleri, C., Mortari, D.: Constellation design using flower constellations. Paper AAS, 04–208 (2004)
7. Mortari, D., Wilkins, M.P., Bruccoleri, C.: The flower constellations (2004)
8. Bruccoleri, C., Mortari, D.: The flower constellations visualization and analysis tool. In: 2005 IEEE Aerospace Conference, pp. 601–606. IEEE (2005)
9. Mortari, D.: Flower constellations as rigid objects in space. *ACTA Futura* **2**, 7–22 (2006)
10. Russell, R.P., Lara, M.: Long-lifetime lunar repeat ground track orbits. *J. Guid. Control, Dyn.* **30**, 982–993 (2007). doi:[10.2514/1.27104](https://doi.org/10.2514/1.27104)
11. Lan, W.: Poly picosatellite orbital deployer Mk III ICD. Preliminary, California Polytechnic State University, San Luis Obispo, CA (2007)
12. Vallado, D.A.: Fundamentals of astrodynamics and applications. Springer (May 2007)
13. Villac, B.F., Scheeres, D.J.: New class of optimal plane change maneuvers. *J. Guid. Control Dyn.* **26**(5), 750–757 (2003)
14. Schaub, H., Alfriend, K.T.: Impulsive feedback control to establish specific mean orbit elements of spacecraft formations. *J. Guid. Control Dyn.* **24**, 739–745 (2001). doi:[10.2514/2.4774](https://doi.org/10.2514/2.4774)
15. Marinan, A.D.: From CubeSats to constellations: systems design and performance analysis. PhD Thesis, Massachusetts Institute of Technology (2013)